# Sudden Frequency Deviations Caused by Solar Flares
# Part I ~ Concepts

Whitham D. Reeve

## 1-1. Introduction

This paper describes sudden frequency deviations of WWV and WWVH time service signals received at Anchorage, Alaska USA from June through December 2014. A Sudden Frequency Deviation (SFD, figure 1) is a change in the received frequency of a fixed carrier caused by rapid changes in Earth's ionosphere from a solar flare. Part I describes the concepts of sudden frequency deviations in terms of solar flares and ionospheric propagation, and Part II describes the instrumentation and observations during the study period.

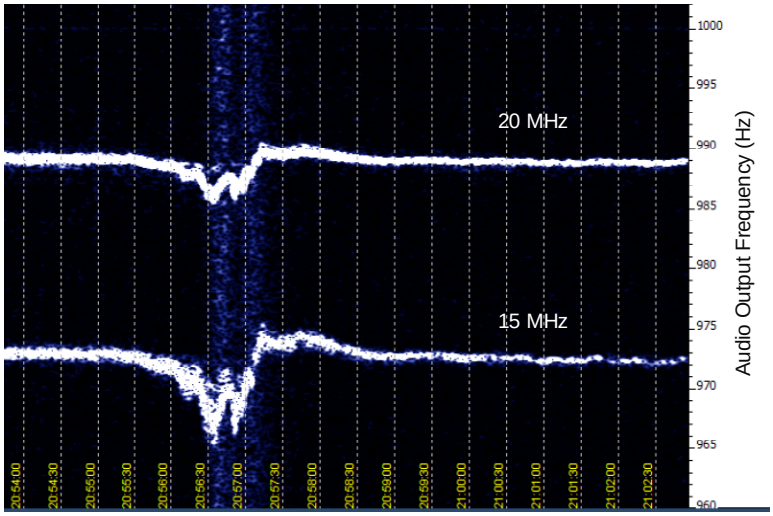


Figure 1 ~ Sudden frequency deviation lasting approximately 3 minutes at on 11 June 2014 related to an M3.9 x-ray flare. The horizontal scale is time in Universal Coordinated Time (UTC) with a 30 s grid, and the vertical scale is the tuned offset of the receiver from the WWV carriers indicated. This SFD had two peaks and maximum frequency deviation of about 7 Hz. The solar flare that caused this SFD included radio bursts covering a very wide frequency range and an optical flare lasting about 30 minutes. A downward shift corresponds to an increase in the received carrier frequency. Image © 2014 W. Reeve.

WWV and WWVH transmit continuous radio frequency carriers with very high accuracy and stability on 2.5, 5, 10 and 15 MHz. WWV also transmits on 20 MHz and in April 2014 restarted transmitting on 25 MHz. The transmitted carrier frequencies are accurate to a few parts in $10^{13}$ (about 0.000 000 000 000 3 Hz). The received short-term accuracy is degraded to a few parts in $10^{9}$ during normal propagation, but sudden frequency deviations lasting a minute or more due to solar flares can be several orders of magnitude worse.

Two ionospheric conditions are attributed to sudden frequency deviations, both caused by the x-ray, extreme ultraviolet and ultraviolet energy released by a solar flare. First, a slab of ionosphere below the reflection region undergoes a rapid change in refraction index and, second, the ionosphere's reflection region undergoes a rapid vertical movement. Both conditions introduce a Doppler shift in the radio wave by changing the effective path length. Either one or both together can cause a sudden frequency deviation.

The method of detecting sudden frequency deviations described here can be quite sensitive. The weakest x-ray flare associated with a detected SFD during the study period was B6.3. However, it was found that stronger x-ray class flares did not always produce an SFD, thus making it clear that the x-ray class of a flare alone does not determine if an SFD is produced. On the other hand, the underlying mechanism that causes a sudden frequency

deviation, a solar flare, also can cause a sudden ionospheric disturbance (SID) at VLF. Therefore, SFD detection may be useful in verifying a SID.

### 1-2. Space Weather Effects

Earth, the near-Earth environment, spacecraft and space travel are affected by the natural conditions and processes in the solar system called space weather. The Sun controls space weather, which includes a wide range of disturbances. Of interest here are disturbances to Earth's ionosphere by the x-ray, extreme ultraviolet and ultraviolet flux from a solar flare (figure 2). These can be manifested as radio blackouts at HF (also called Short Wave Fadeout, SWF) and the familiar sudden ionospheric disturbances (SID) at VLF. Less well-known, and the subject of this paper, are the sudden frequency deviations caused by rapid changes of the ionosphere's electron density and height that cause easily detectable Doppler shifts in terrestrial carrier frequencies. SFDs were extensively studied in the 1960s as a means to detect solar flares ("solar flare patrol") [Agy]. Probably even less well known, and beyond the scope of this paper, are additional solar flare manifestations: Sudden Phase Disturbance (SPD) or Sudden Phase Anomaly (SPA), Sudden Cosmic Noise Absorption (SCNA), Sudden Enhancement of Atmospherics (SEA), Sudden Increase in Total Electron Content (SITEC), and Geomagnetic Solar Flare Effect (GSFE) to name a few.

Note: Links in braces { } and references in brackets [ ] are provided in **section 1-6**.

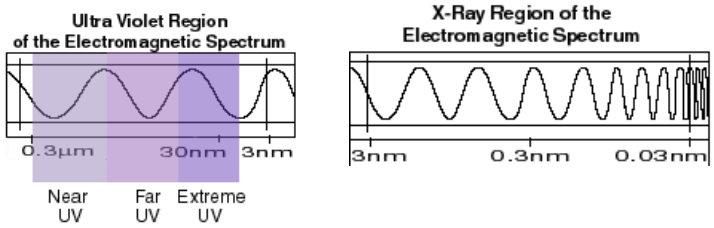


Figure 2 ~ Ultraviolet, extreme ultraviolet and x-ray wavelengths range from approximately 0.3 µm to 0.03 nm. Images courtesy NASA.

### 1-3. Solar Flares

Solar flares (figure 3) are *intense bursts of radiative energy across the entire electromagnetic spectrum, with the large burst enhancements in the X-ray, extreme ultraviolet (EUV) and radio portions of the spectrum* [Knipp]. The radiations occur on a time scale of minutes as electrons and other charged particles accelerate to high energies at or near the site where the Sun's magnetic field lines merge during a process called reconnection. *Most manifestations of solar flares seem to be secondary responses to the original energy release process, converting magnetic energy into particle energy, heat, waves, and motion* [Benz]. These interactions produce the radiation detected about eight minutes later at Earth. Like sudden ionospheric disturbances, sudden frequency deviations are indirect effects of a solar flare, and their detection is through flare effects on radio propagation and not of the flare itself.

The Space Weather Prediction Center (SWPC) daily Events List {EVENTS} shows solar activity detected and measured by a variety of terrestrial and spacecraft sensors. X-ray events, shown in the Events List under the XRA type designation, are reported by the GOES spacecraft and are assigned an x-ray class based on the measured peak flux (table 1). Many XRA events also produce optical flares observed in H-alpha line wavelength (656 nm).

Optical flares are given the FLA type designation in the Events list and are classified by importance and brightness (table 2).

Table 1 ~ X-ray classes reported by Space Weather Prediction Center using GOES spacecraft data in the 0.1 to 0.8 nm wavelength range

| Class | x = Peak flux ($W/m^2$) |
|---|---|
| A | $x < 10^{-7}$ |
| B | $10^{-7} \le x < 10^{-6}$ |
| C | $10^{-6} \le x < 10^{-5}$ |
| M | $10^{-5} \le x < 10^{-4}$ |
| X | $10^{-4} \le x$ |

Table 2 ~ Optical flare *importance* and *brightness* levels reported by Space Weather Prediction Center. Importance is the corrected area of the flare in heliospheric square degrees at maximum brightness observed in the H-alpha line wavelength (656 nm)

| Importance | Area (square degrees) |
|---|---|
| S (Subflare) | ≤ 2.0 |
| 1 | 2.1 ≤ x < 5.1 |
| 2 | 5.2 ≤ x < 12.4 |
| 3 | 12.5 ≤ x < 24.7 |
| 4 | ≥ 24.8 |
| **Brightness** | **Relative maximum brightness** |
| F | Faint |
| N | Normal |
| B | Brilliant |

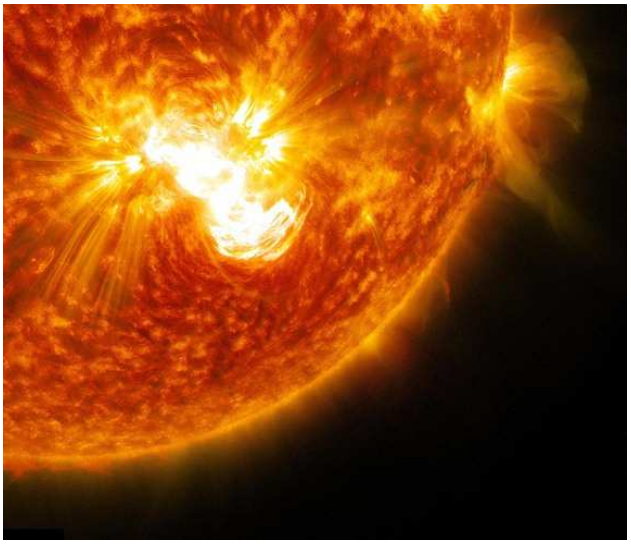

Figure 3 ~ X3.1 x-ray class solar flare (bright region) on 24 October 2014 imaged at extreme ultraviolet wavelengths. Image courtesy NASA/SDO.

### 1-4. Ionospheric Propagation

Energy radiated by an HF transmitter such as a WWV transmitter is propagated to a distant receiver by ground waves or sky waves (figure 4). Ground waves follow Earth's surface and generally have a maximum range of several hundred kilometers. On the other hand, sky waves involve one or more reflections (or hops) between Earth's ionospheric regions and surface or even between regions (see sidebar below). In principle the maximum distance for 1-hop sky wave propagation is about 5000 km, which corresponds to a reflection height above Earth of roughly 500 km, but in practice the maximum distance is closer to 4000 km, corresponding to approximately 300 km reflection height. Propagation to a distance station may involve more than one hop even if the distance is < 4000 km. For detailed technical discussion on ionospheric radio propagation, see [Davies] or [Fabrizio].

If the radio propagation conditions are constant, a fixed receiver will receive the same frequency as radiated by a fixed transmitter. However, the ionosphere is like an upside-down water pool being tilted and stirred by winds and swimmers. The ionosphere continuously changes over short and long time periods depending on solar activity, sunrise and sunset, daytime and nighttime and high altitude winds. These changes ordinarily are relatively slow and do not affect the received frequency in any abrupt way. On the other hand, large rapid changes can cause measurable Doppler shifts.

The great circle distance between the WWV station near Boulder, Colorado and Anchorage is approximately 3800 km and from WWVH near Kekaha on Kauai, Hawaii is approximately 4400 km (figure 5). The Boulder route is mostly over land and the Kauai route is almost entirely over sea water; the latter having better HF reflection characteristics for multi-hop propagation. Both transmitting stations are near the maximum distance for 1-hop propagation, so two or more hops likely were involved during the live measurements described in this paper. Simultaneous reception of multiple hop modes using multiple refection regions (figure 6) may explain some of the anomalies that I observed at various times. Assuming a (typical) reflection region height of 250 km, the path lengths and elevation angles are shown in table 3.


**Ionospheric reflection and refraction**: Reflection is the term most easily understood and most often used to describe a sky wave that is directed upward and returns to another point on Earth; however, refraction is the primary method by which an oblique radio wave is returned as it passes through ionospheric regions and is bent downward by the varying index of refraction in those regions. On the other hand, reflection can occur when the wave vertically enters the

Figure 4 ~ Ground wave and sky wave propagation concepts. A 2-hop sky wave path and a ground wave path are shown for illustration, but ground wave propagation from the WWV transmitter to Anchorage is highly improbable because of the distance (about 3800 km). Underlying map image courtesy Google Earth.

The sudden increase in x-ray and EUV radiation during a solar flare increases the rate of electron production in Earth's ionosphere, in particular in the E-and F-regions at altitudes above approximately 100 km. The increased electron density further speeds up the rate of electron loss (electron loss occurs when the electrons recombine with ions), but if the net increase is rapid enough, a sudden frequency deviation occurs. According to [Agy] most SFD observations are on radio paths reflected from the F-region of the ionosphere but they also may be reflected from the E-region. He states that SFDs observed on paths reflected from the bottom of the E -region or

from sporadic-E are generally smoother, slower, and much smaller than those observed on paths reflected from the F-region.

Figure 5 ~ Great circle maps for propagation between Boulder, Colorado (below, indicated as WBU) and Anchorage (ANC) and between Kauai, Hawaii (right, LIH) and Anchorage. Maps are from Great Circle Mapper {GCM}.


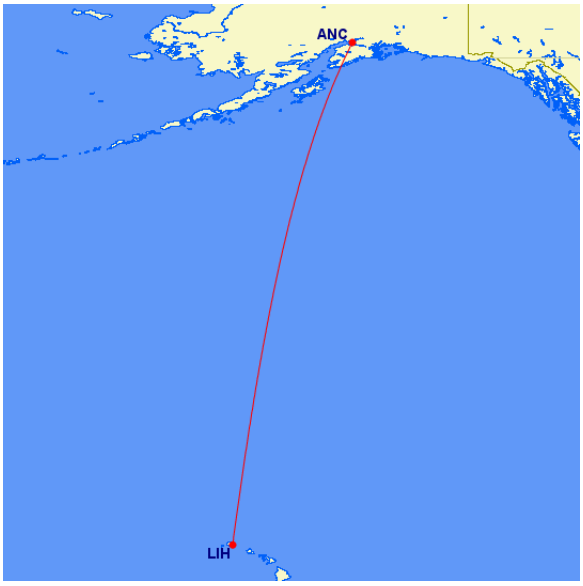


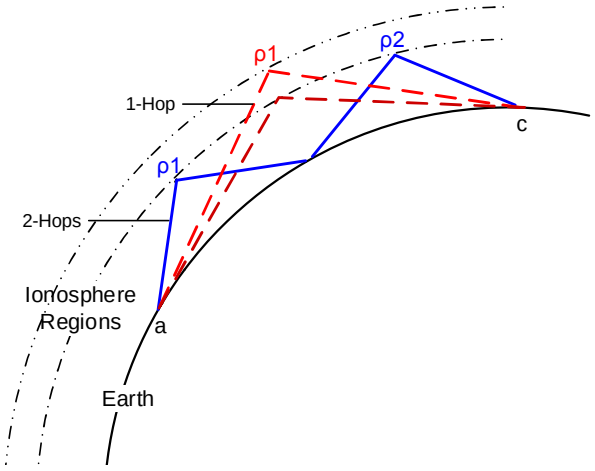


Figure 6 ~ Schematic of 1-hop (red trace) and 2-hop (blue) modes between terrestrial points a and c. The ionospheric regions are indicated by dotted-dashed lines. The 1-hop mode is shown for two different reflection heights. The elevation angle of the radio propagation path increases as the modes increase for any pair of end points. Simultaneous reception of more than one mode or modes with different reflection heights may have been involved at various times throughout the period discussed in this paper. Image © 2014 W. Reeve

Table 3 ~ Modes, total path lengths and elevation angles for sky wave propagation from Boulder to Anchorage (3800 km great circle distance) assuming 250 km reflection height. These parameters were calculated using techniques described in [SSFD].

| Hops | Total path length (km) | Elevation angle ( ° ) |
|---|---|---|
| 1 | 3892 | 1.2 |
| 2 | 3997 | 10.2 |
| 3 | 4153 | 18.3 |
| 4 | 4359 | 25.2 |

## 1-5. Sudden Frequency Deviations

Sudden frequency deviations were first described in 1960 in [Watts]. As reported in [Agy] in 1965, sudden frequency deviations are generally characterized by a rapid positive frequency shift followed immediately by a smaller negative frequency shift and a gradual recovery to pre-flare conditions (figure 7 and 8). Their shape, duration and magnitude vary considerably from flare-to-flare. Not all SFDs show the negative frequency shift during recovery and they often have more than one peak. The peak frequency deviation usually occurs within 1 or 2 minutes and varies from a few tenths to tens of hertz. The total duration varies from less than a minute to ten minutes or more.

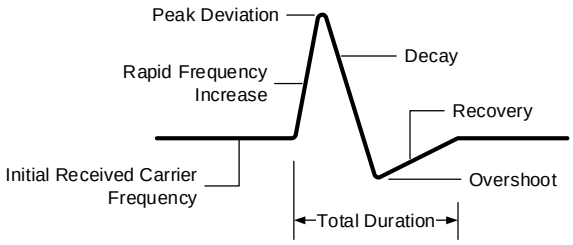


Figure 7 ~ Schematic of a typical sudden frequency deviation. Many variations have been observed including double peaks, no overshoot, and follow-on frequency deviations (ripple). Image © 2014 W. Reeve

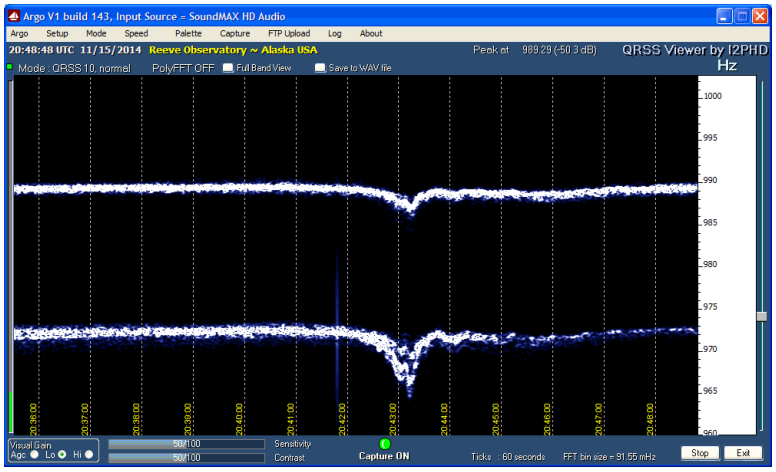


Figure 8 ~Textbook sudden frequency deviations at 15 MHz (lower) and 20 MHz (upper) on 15 November 2014. Radio blackout conditions at 15 MHz progressed after the flare. Image © 2014 W. Reeve

Most SFDs are shorter than the duration of the flare that caused it. It was found in early studies that the peak frequency deviation occurred 1 to 4 minutes before the flare optical peak, and that more SFDs are detected near local solar noon than other times of the day. Not all solar flares cause an SFD but, when they do, the stronger the flare the more likely it will cause a higher frequency shift. Only 13% of all optical flares caused an SFD in a 1962 study [Agy]. It should be noted that this study took place when flares were measured only by their optical importance and not also by their x-ray class.

Other early studies clearly showed that a number of variables are involved in correlating the deviations with solar flares. Interestingly, the season is not one of them, but some variables that do have an effect are:

- Carrier frequency
- Propagation path characteristics
- Solar flare importance and other flare characteristics
- Level of solar activity (solar cycle)
- Time of day
- Geomagnetic latitudes of transmitting and receiving stations

Assuming both transmitter and receiver are fixed, two basic conditions can affect the received frequency as mentioned above: (1) Change in the ionosphere's refractive index as a result of change in electron density; and (2) Change in the path length due to rapid vertical movement of the radio wave's ionospheric reflection region. In both conditions, there is a change in the phase path between the transmitter and receiver. When the phase path starts to decrease the received frequency increases, and when the phase path starts to increase the received frequency decreases. It is possible for both electron density changes and path length changes to exist simultaneously, but studies have shown that **Condition (2)** is more common [Davies].

The following analyses are based on work described in [Davies] and others. Physical interpretations will be provided as the equations are developed. Out of necessity of presentation, these analyses make simplifying assumptions.

The wavelength λ of a radio wave in a refractive medium like the ionosphere is given by

$$\lambda = \frac{c}{n \cdot f} \tag{1}$$

where
λ = wavelength or radio wave in the medium (m)
c = speed of light in a vacuum ( $3 \cdot 10^8$ m/s)
n = index of refraction of the medium
f = frequency (Hz)

The index of refraction (or refractive index) of a medium is the ratio of the speed of light in a vacuum to its speed in the medium (it is equivalent to the inverse of velocity factor that is used to calculate coaxial transmission line lengths). The number of waves P on a path of length s is

$$P = \frac{s}{\lambda} \tag{2}$$

The path can consist of one or more hops and s is the total of all hops. The frequency deviation $\Delta f$ of the received signal is the time derivative of the number of waves P, or

$$\Delta f = -\frac{d}{dt}(P) = -\frac{d}{dt}\left(\frac{s}{\lambda}\right) \tag{3}$$

The negative sign results because $\Delta f$ changes oppositely to the rate of change of P. That is, the path length may increase or decrease and the rate of change of the path length is equivalent to the transmitter moving away from or toward the receiver, respectively. The change produces the familiar Doppler effect in which the received signal frequency decreases or increases with respect to the transmitted signal frequency.

As a signal passes through a medium with refractive index n, such as the ionosphere, it slows to speed v according to

$$v = \frac{c}{n} \tag{4}$$

A radio wave takes longer to pass through the medium than through a vacuum, giving the appearance of a longer path. The time along the apparent path $s_a$ is

$$t = \frac{s_a}{c} \tag{6}$$

The propagation time along the actual path s is

$$t = \frac{s}{v} = \frac{n \cdot s}{c} \tag{5}$$

Combining equation (5) and equation (6) gives the apparent path in terms of the actual path, or

$$s_a = n \cdot s \tag{7}$$

Rearranging and combining equations (1), (3) and (7) gives the frequency change, or Doppler shift, in terms of the rate of change of apparent path length, or

$$\Delta f = -\frac{f}{c} \cdot \frac{ds_a}{dt} \tag{8}$$

Both n and s are functions of time; therefore, differentiating equation (7) with respect to time gives

$$\frac{ds_a}{dt} = n \cdot \frac{ds}{dt} + s \cdot \frac{dn}{dt} \tag{9}$$

Substituting the right side of equation (9) in equation (8) gives

$$\Delta f = -\frac{f}{c} \cdot \left[ n \cdot \frac{ds}{dt} + s \cdot \frac{dn}{dt} \right] \tag{10}$$

Equation (10) shows the two conditions mentioned at the beginning of this section. First, if the path length s is constant, then

$$\frac{ds}{dt} = 0$$

and the change in frequency is given by

$$\Delta f = -\frac{f}{c} \cdot \left[ s \cdot \frac{dn}{dt} \right] \tag{11}$$

Similarly, if the refractive index is constant, then

$$\frac{dn}{dt} = 0$$

and the change in frequency is given by

$$\Delta f = -\frac{f}{c} \cdot \left[ n \cdot \frac{ds}{dt} \right] \tag{12}$$

The first condition – change in refractive index – can be modeled as extra ionization in a "slab" of ionosphere below the reflection region (figure 9). The second condition – change in path length – can be modeled as extra ionization in the F-region causing apparent up or down movement of the reflection region. Note that it is the rate of change of ionization not just a change in the ionization that causes these conditions.

Further analysis of the illustrated conditions provides additional details for interpretation. For the slab ionosphere condition – **Condition (1)** – the change in the apparent path $\Delta s_a$ of the radio wave in both directions (up through the slab to the reflection region and back down through the slab) with respect to the change in refractive index $\Delta n$ is

$$\Delta s_a = 2 \cdot \Delta n \cdot \frac{D}{\sin\theta} \tag{13}$$

where
D = thickness of the D-region ionosphere below the reflective E- and F-regions (m)
$\theta$ = elevation angle of propagation path (rad)

Substituting equation (13) in equation (8) gives

$$\Delta f = -2 \cdot \frac{f}{c} \cdot \frac{D}{\sin\theta} \cdot \frac{dn}{dt} \tag{14}$$

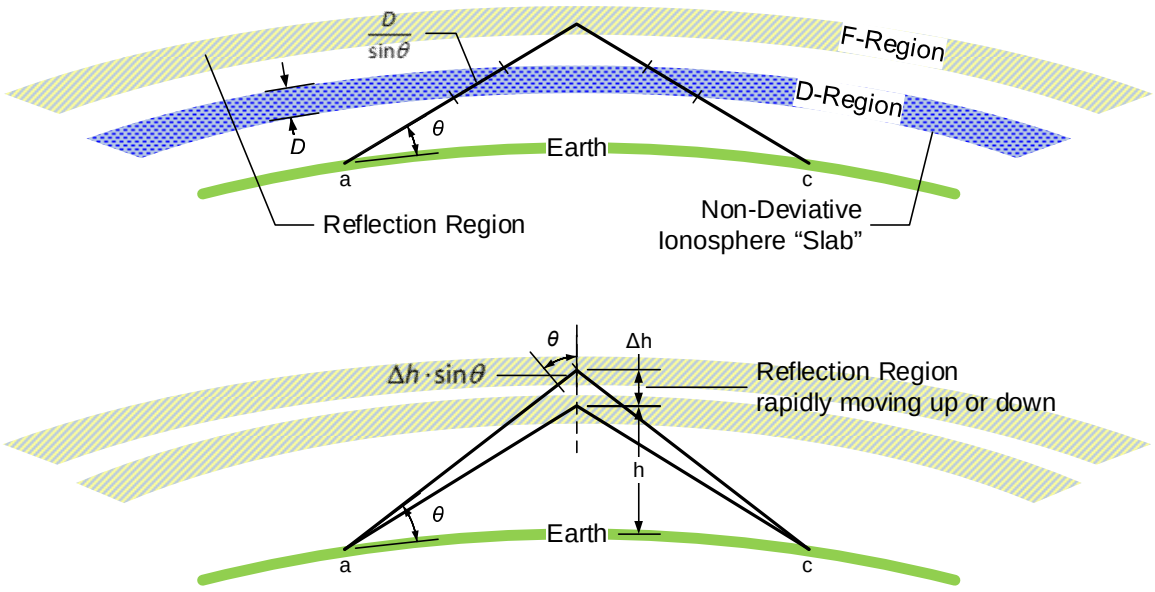


Figure 9 ~ Ionospheric reflection configurations related to sudden frequency deviations. Upper: **Condition (1)** – Slab of ionosphere in which the refraction index rapidly changes. Lower: **Condition (2)** – Rapid vertical movement of the ionosphere's reflection region. Image © 2014 W. Reeve

To simply this analysis, the effects of the geomagnetic field and collisions between electrons and neutral particles are ignored. In this case [Davies],

$$n^2 = 1 - \frac{k \cdot N}{f^2} \tag{15}$$

where

N = electron density (electrons/$m^3$) (figure 10)

k = $e^2 \Big/ \left[ 4 \cdot \pi^2 \cdot \varepsilon_0 \cdot m \right]$ (= 80.5 $m^3/s^2$) (do not confuse this k with the Boltzmann constant)

$\varepsilon_0$ = permittivity of free space ( $8.85 \cdot 10^{-12}$ F/m = $8.85 \cdot 10^{-12}$ $s^2C^2/m^3kg$ )

e = electron charge ( $1.6 \cdot 10^{-19}$ C)

m = electron mass ( $9.11 \cdot 10^{-31}$ kg)

When the electron density increases in a layer in which the refractive index n is close to unity (called a *non-deviative* region because there is no appreciable refraction of the radio wave and, thus, no deviation in the path direction), equation (15) can be factored, or

$$n^2 = 1 - \frac{k \cdot N}{f^2} \approx \left( 1 - \frac{k}{2} \cdot \frac{N}{f^2} \right)^2 = 1 - \frac{k \cdot N}{f^2} + \left( \frac{k}{2} \cdot \frac{N}{f^2} \right)^2 \tag{16}$$

The last term in equation (16) is very small compared to the other terms and can be ignored. Therefore, n can be approximated by

$$n \approx \sqrt{\left( 1 - \frac{k}{2} \cdot \frac{N}{f^2} \right)^2} \approx 1 - \frac{k}{2} \cdot \frac{N}{f^2} \tag{17}$$

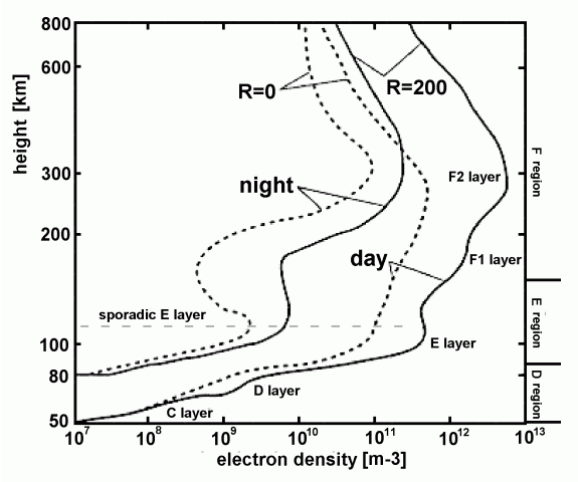


Figure 10 ~ Typical ionospheric electron density (N) profiles with annotations for day/night and low/high monthly median solar index (R). Solid lines: Sunspot maximum (R=200); Dashed lines: Sunspot minimum (R=0). The horizontal scale indicates the amount of ionization of the atmosphere in terms of the electron density (number of electrons per cubic meter volume) as the height changes on the left vertical scale. For example, the peak F2-region density during the day at the peak of the solar cycle almost $10^{13}$ electrons per cubic meter and occurs at a height of around 300 km. The right vertical scale shows the approximate heights of each ionospheric region. Underlying image source: [Hunsucker, figure 1.4]

A small change in refractive index $\Delta n$ due to a small change in electron density $\Delta N$ is

$$n + \Delta n \approx 1 - \frac{k}{2} \cdot \frac{N + \Delta N}{f^2} \tag{18}$$

Solving for $\Delta n$

$$\Delta n \approx \left( 1 - \frac{k}{2} \cdot \frac{N + \Delta N}{f^2} \right) - n = \left( 1 - \frac{k}{2} \cdot \frac{N + \Delta N}{f^2} \right) - \left( 1 - \frac{k}{2} \cdot \frac{N}{f^2} \right) = -\frac{k}{2} \cdot \frac{\Delta N}{f^2} \tag{19}$$

Substituting equation (19) into (14) gives

$$\Delta f = \frac{k}{c \cdot f} \cdot \frac{D}{\sin\theta} \cdot \frac{dN}{dt} \tag{20}$$

From equation (20), for the condition where the electron density changes in a non-deviative ionospheric slab below the reflection region, the frequency deviation is inversely proportional to both the transmitter frequency and sine of the elevation angle. That is, for a given set of conditions the frequency deviation at, say, 20 MHz will be lower than at, say, 15 MHz. It should be noted that the increased electron density in the non-deviative region can impose considerable attenuation through absorption of the radio wave.

For the condition where the reflection region moves up or down – **Condition (2)** – the analysis follows a similar sequence. Where *h* is the reflection height, $\Delta h$ is the change in reflection height and $\Delta h << h$ , the change in the apparent path length is

$$\Delta s_a = 2 \cdot \Delta h \cdot \sin\theta \tag{21}$$

Substituting equation (21) in (8) gives

$$\Delta f = -2 \cdot \frac{f}{c} \cdot \frac{dh}{dt} \cdot \sin\theta \tag{22}$$

Therefore, for the condition where the reflection height moves up or down, the frequency deviation is proportional to both frequency and sine of the elevation angle. That is, for a given set of conditions the frequency deviation at, say, 20 MHz will be higher than at, say, 15 MHz.

The above analyses assume no geomagnetic field effects and no energy losses (absorption) through collisions. In general, a magnetic field in an ionized medium causes a linearly polarized wave to split into two components, *ordinary* and *extraordinary*, a process called *magneto-ionic splitting* (see chapter 2 in [Fabrizio]). The two waves have elliptical polarizations that rotate in opposite directions, and the two waves are refracted different amounts as they propagate through the ionosphere so they follow slightly different paths and have slightly different absorption and velocities. If the original wave's electric field is aligned with the geomagnetic field, there are no effects. Otherwise, the relative amplitude of the extraordinary wave depends on the relative orientation of the magnetic field with respect to the radio wave's plane of polarization and the magnetic field's strength. Amplitude is highest when the electric field is perpendicular to the magnetic field.

As a radio wave passes through the ionosphere, it causes electrons to vibrate and these electrons occasionally collide with neutral gas molecules. The energy that the electrons acquired from the radio wave is thus lost from the radio wave. The amount of energy absorbed in this manner depends on the atmospheric gas pressure, velocity that the electron acquires in its vibrations and the electron density. The gas pressure in the ionosphere increases as altitude decreases, so the highest energy loss, or absorption, is in the D-region of the ionosphere. The ionosphere has some conductivity but also behaves like a dielectric with a dielectric constant less than unity. These factors are different for the ordinary and extraordinary waves previously described.

For the condition where the radio wave passes thru an ionospheric slab below the reflection region, the splitting into ordinary and extraordinary waves has some effect; however, for the condition where the reflection point moves up and down, it has no effect.

While the above analyses make several simplifying assumptions and the effects of the geomagnetic field and absorption are not quantified, it still is possible to draw some general conclusions

- ☼ The frequency deviation is proportional to the time rate of change of the effective path length
- ☼ The path length can be affected by electron density change in both a non-deviative ionosphere slab below the reflection region and in the reflection region itself
- ☼ The more rapid the change in electron density, the larger the frequency deviation
- ☼ The frequency deviation is inversely proportional to the carrier frequency when the phase path is altered in the non-deviative ionosphere slab and proportional to the carrier frequency when the phase path is altered at the reflection region
- ☼ SFD measurements provide some basic information about the ionosphere and how solar flares affect it

## 1-6. References, Further Reading and Web Links for Part I


References:

[Agy] Agy, V., Baker, D., Jones, R., Studies of Solar Flare Effects and Other Ionospheric Disturbances with a High Frequency Doppler Technique, Technical Note 306, National Bureau of Standards, 28 Apr 1965

[Benz] Benz, A., Flare Observations, Living Review Solar Physics, 5, 2008

[Davies] Davies, K., Ionospheric Radio Propagation, Dover Publications, 1966

[Fabrizio] Fabrizio, G., High Frequency Over-The-Horizon Radar, McGraw-Hill Book Co., 2013

[Hunsucker] Hunsucker, R. and Hargreaves, J., The High-Latitude Ionosphere and Its Effects on Radio Propagation, Cambridge University Press, 2007

[Knipp] Knipp, D., Understanding Space Weather and the Physics Behind It, McGraw-Hill Book Co., 2011

[Watts] Watts, J. and Davies, K., Rapid Frequency Analysis of Fading Radio Signals, Journal of Geophysical Research, Vol. 65, No. 8, 2295-2301, August 1960

Further Reading:

[Baker] Baker, D., A Comparison of Sudden Ionospheric Frequency Deviations with Solar X-ray and Centimeter-Wave Emission During October 1963, Environmental Science Services Administration Technical Report IER 43 – ITSA 43, September 1967

[Gassmann] Gassmann, G., Editor, The Effect of Disturbances of Solar Origin on Communications, The Macmillan Company, 1965

[Huijun] Huijun, L., Libo, L., Chen, B., Jiuhou, L., Xinan, Y., Weixing, W., Modeling the Response of the Middle Latitude Ionosphere to Solar Flares, Journal of Atmospheric and Solar-Terrestrial Physics, Vol. 69, 2007, pg 1587-1598

[Liu] Liu, J., Chiu, C., Lin, C., The Solar Flare Radiation Responsible for Sudden Frequency Deviation and Geomagnetic Fluctuation, Journal of Geophysical Research, Vol. 101, No. A5, pg 10,855-10,862 (paper no. 95JA03676)

[Watanabe] Watanabe, D., Nishitani, N., Study of Ionospheric Disturbances During Solar Flare Events Using the SuperDARN Hokkaido Radar, Advances in Polar Science, Vol. 24, No. 1: 12-18, March 2013

Web Links:

{EVENTS} ftp://ftp.swpc.noaa.gov/pub/indices/events/

{GCM} http://www.gcmap.com/

**Document Information**

Author: Whitham D. Reeve



Revisions:
- 0.0 (Original draft started, 12 Jun 2014)
- 0.1 (additions to 1st draft, 16 Jun 2014)
- 0.2 (Edits to 1st draft, 28 Jun 2014)
- 0.3 (Numerous additions and split into parts I and II, 11 Jul 2014)
- 0.4 (Edits to split into 2 parts, 31 Jul 2014)
- 0.5 (Edits to part 1, 28 Sep 2014)
- 0.6 (Split into 2 parts prior to data reduction, 25 Dec 2014)
- 0.7 (Continuation of Part I, 17 Jan 2015)
- 0.8 (Completion of 1st draft, 18 Jan 2015)
- 0.9 (Minor revisions, 21 Jan 2015)
- 1.0 (Completion of 2nd draft, 23 Jan 2015)
- 1.1 (Added solar images, 27 Jan 2015)
- 1.2 (Minor additions to section 1-5, 24 Mar 2015)

Word count: 4218

File size (bytes): 3408384